Reprinted from the Journal of the American Ceramic Society, Vol. 70, No. 4, April 1987

Crack-Interface Grain Bridging as a Fracture Resistance Mechanism in Ceramics: II, Theoretical Fracture Mechanics Model

YIU-WING MAI† and BRIAN R. LAWN*

Ceramics Division, National Bureau of Standards, Gaithersburg, Maryland 20899

A fracture mechanics model is developed for nontransforming ceramics that show an increasing toughness with crack extension (*R*-curve, or *T*-curve, behavior). The model derives from the observations in Part I, treating the increased crack resistance as the cumulative effect of grain bridging restraints operating behind the advancing tip. An element of discreteness is incorporated into the formal distribution function for the crack-plane restraining stresses, to account for the primary discontinuities in the observed crack growth. A trial force-separation function for the local bridge microrupture process is adopted, such that an expression for the microstructure-associated crack driving (or rather, crack closing) force may be obtained in analytical form. The description can be made to fit the main trends in the measured toughness curve for a coarse-grained alumina. Parametric evaluations from such fits conveniently quantify the degree and spatial extent of the toughening due to the bridging. These parameters could be useful in materials characterization and design. It is suggested that the mechanics formulation should be especially applicable to configurations with short cracks or flaws, as required in strength analysis.

Presented at the 88th Annual Meeting of the American Ceramic Society, Chicago, IL, April 30, 1986 (Basic Science Division, Paper No. 166-B-86). Received April 16, 1986; revised copy received September 2, 1986; approved October 14, 1986.

Supported by the U.S. Air Force Office of Scientific Research; support for Y.-W. M. provided by the NBS Guest Worker Program.

*Member, the American Ceramic Society.

†On leave from the Department of Mechanical Engineering, University of Sydney, N.S.W. 2006, Australia.

I. Introduction

WE HAVE presented direct experimental evidence in Part I for a mode of crack restraint by grain-localized interfacial bridging behind the advancing tip.[1] The suggestion was made that this mode of restraint is probably a dominant mechanism of *R*-curve behavior in ceramics, at least in nontransforming ceramics. Consequently, there is a need to develop a suitable fracture mechanics model, to establish a sound basis for materials design.

This need constitutes the primary driving force for Part II of our study. We shall derive a formulation for the crack resistance as an increasing function of crack size, bounded in the lower limit by some intrinsic toughness (determined by bulk cleavage or grain boundary energies) and in the upper limit by the macroscopic toughness (representative of the microstructural composite). Following Part I, we shall again take coarse-grained alumina as our representative material, using the measured scaling dimensions for the interfacial bridging process as a basis for quantitative analysis of the observed *R* curve (or, as we shall come to call it, the *T* curve). In setting up our model we will be particularly mindful of the discontinuous (yet highly stable) nature of the crack growth during the loading to failure, most notably in the strength configurations.[1] Speaking of strength configurations, the present analysis supersedes that described in an earlier study using controlled flaws,[2,3] where the microstructural contribution to the fracture mechanics was introduced empirically without reference to any specific toughening mechanism.

An important feature of our modeling will be the capacity for separating out the fracture mechanics from the material characteristics. Essentially, our formalism requires us to specify a local force-separation relation for the restraining interfacial ligaments.

Our observations in Part I provide little clue as to what fundamental material quantities should appear in this relation, but they contain some indications as to the *form* (i.e., pronounced tail) and *spatial extent* (i.e., as determined by the critical bridging dimensions referred to above) of the functional dependence. It is thus inevitable that our treatment, while structured on a well-confirmed physical separation model, will retain an element of empiricism. We shall make use of precedents set elsewhere in deciding on an appropriate function for our alumina. This approach will preclude us from making a priori predictions of R-curve behavior in *other* materials. Accordingly, questions as to why R-curve behavior is so variable from material to material (even for materials of the same nominal composition, differing only in the grain boundary structures),[2,3] are posed as important topic areas for future researchers. Conversely, our formulation will enable us to describe the complete crack resistance behavior for a given material without explicit knowledge of the fundamental underlying separation relations.

Once again, let us foreshadow one of the ultimate goals of our study, to account for the anomalous strength characteristics shown by materials with strong R-curve behavior.[2,3] In this paper we shall confine ourselves to *qualitative* explanations of some of the more distinctive features of the crack response from indentation flaws, namely, the relative insensitivity of failure stress to flaw size at low loads and the associated growth discontinuities. A detailed quantitative treatment of the problem, in which the indentation-strength data are inverted to obtain the R curve, will be given elsewhere.[4]

II. Interfacial Crack Restraint Model

In this section we develop a fracture mechanics model for a crack restrained at its newly formed interface by distributed closure forces. These closure forces are identified with unruptured bridges whose specific nature is determined by the ceramic microstructure. As such, the restraint is analogous to that considered in the fiber-reinforced ceramic composite models,[5–7] although the underlying microstructural rupture mechanisms in the monophase materials of primary interest here may be of an entirely different kind. We shall begin with a general statement of the crack resistance problem and progressively introduce factors specific to the processes described in Part I.

(1) General Statement of Crack Resistance Problem

Our analysis here is based on equilibrium fracture mechanics, i.e., on the Griffith notion that a crack is on the verge of extension when the net mechanical driving force on the system is just equal to the intrinsic resistance (toughness) of the material.[8] The equilibrium can be stable or unstable, depending on the crack-size variation of the opposing force terms. The terminology "R curve" derives from energy release rate (G) considerations, where $R = R(c)$ is the crack-size-dependent fracture surface energy of the material. Here we shall work instead with stress intensity factors (K) because of their simple linear superposability, replacing R with an analogous toughness parameter $T = T(c)$: hence our preference for the term "T curve".[9]

Our starting point is a general expression for the net stress intensity factor for an equilibrium crack:[9]

$$K = K_a + \sum_i K_i = T_0 \tag{1}$$

$K_a = K_a(c)$ is the familiar contribution from the applied loading. The terms $K_i = K_i(c)$ represent contributions from any "internal" forces that might act on the crack, such as the microstructure-associated forces that we seek to include here. T_0 is taken to be the intrinsic material toughness (i.e., the effective K_{IC} for bulk cleavage or grain boundary fracture), strictly *independent of crack size*. Of the individual K terms in Eq. (1) it is only K_a which is monitored directly, via the external loading system, in a conventional fracture test. Consequently, it has become common practice to regard the K_i terms implicitly as part of the toughness characteristic. This philosophy is formalized by rewriting Eq. (1) in the form[9]

$$K_a = T = T_0 - \sum_i K_i \tag{2}$$

The quantity $T = T(c)$ defines the effective toughness function, or T curve. To obtain a rising T curve, the $K_i(c)$ functional dependencies must be either positive decreasing or negative increasing.

The existence of a rising T curve introduces a stabilizing influence on the crack growth. We have alluded to such stabilization repeatedly in Part I. From Eq. (1), the condition for the equilibrium to remain stable is that $dK/dc < 0$[9] (recalling that $dT_0/dc = 0$). Conversely, the condition for instability is that $dK/dc > 0$ (although satisfaction of this condition does not always guarantee failure; see Section IV). In terms of Eq. (2) the corresponding stability/instability conditions are expressible as $dK_a/dc \leqslant dT/dc$. This latter forms the basis for the conventional T-curve (R-curve) construction.

(2) Microstructure-Associated Stress Intensity Factor

Now let us consider the way in which the microstructural crack restraining forces may be folded into the fracture mechanics description. Specifically, we seek to introduce the effect of restraining bridges behind the growing crack tip as an internal stress intensity factor $K_i = K_\mu$. We shall focus specifically on line cracks in this paper, although this should not be seen as restricting the general applicability of the approach.

The configuration on which our model is to be based is shown in Fig. 1. The interfacial bridging ligaments are represented by the array of force centers (circles) projected onto the crack plane. (This array is depicted here as regular but in reality of course there will be a degree of variability in the distribution of centers.) Here c is the distance from the mouth to the front of the crack and d is the mean separation between closure force centers. Note that at very small crack sizes, $c < d_0$, where d_0 is the distance to the *first* bridge (not *necessarily* identical with d; see Section III), the front encounters no impedance. As the front expands, bridges are activated in the region $d_0 \leq x \leq c$. These bridges remain active until, at some critical crack dimension c^* ($\geqslant d$), ligamentary rupture occurs at those sites most remote from the front. Thereafter a steady-state activity zone of length $c^* - d_0$ simply translates with the growing crack.

This configuration would appear to have all the necessary ingredients to account for the most important features in the crack response observed in Part I. The enhanced stability arises from the increasing interfacial restraint as more and more bridging sites are activated by the expanding crack. The discontinuous nature of the growth follows from the discreteness in the spatial distribution of closure forces at the crack plane. Thus the initial crack may become trapped at first encounter with the bridge energy barriers. If these barriers were to be sufficiently large the entire crack front could be retarded to the extent that, at an increased level of applied stress, the next increment of advance would occur unstably to the second set of trapping sites (pop-in). With further increase in applied stress the process could repeat itself over successive barriers, the jump frequency increasing as the expanding crack encompasses more sites within its front. There is accordingly a smoothing out of the discreteness in the interfacial restraints as the crack grows larger until ultimately, at very large crack sizes, the distribution may be taken as continuous.

In principle, we should be able to write down an appropriate stress intensity factor for any given distribution of discrete restraining forces of the kind depicted in Fig. 1. Unfortunately, the formulation rapidly becomes intractable as the number of active restraining elements becomes larger. To overcome this difficulty we resort to an approximation, represented in Fig. 2, in which the summation over discrete forces $F(x)$ is replaced by an integration over continuously distributed stresses $p(x) = F(x)/d^2$. These stresses have zero value in the region $x < d_0$, reflecting the necessary absence of restraint prior to intersection of the first bridging sites. They have nonzero value in the region $d_0 < x < c$ up to the crack size at which ligamentary rupture occurs ($d_0 \leq c \leq c^*$), and thereafter in the region $d_0 + c - c^* < x < c$ where a steady-state configuration obtains ($c > c^*$). This approximation is tantamount to ignoring all but the first of the discontinuous jumps in the

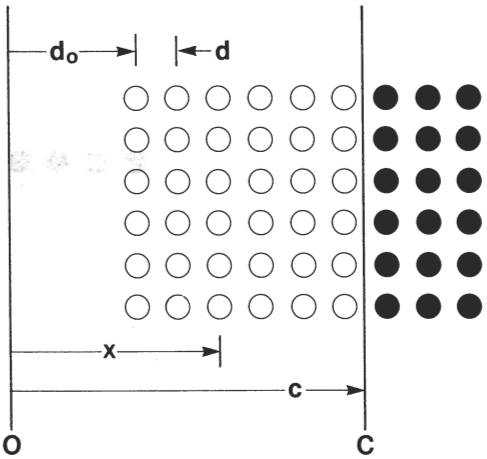

Fig. 1. Schematic of bridging model. *O* denotes origin, *C* front, of crack. Circles indicate bridges; open circles denote active sites, closed circle potential sites.

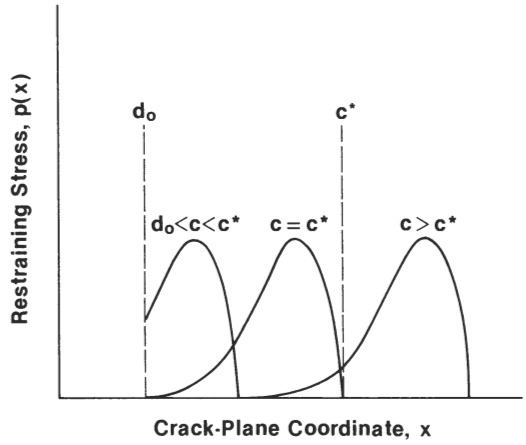

Fig. 2. Representation of bridging restraint over crack plane by continuous closure stress distribution. Distributions shown for three crack lengths c relative to d_0 and c^* (see Fig. 1).

observed crack evolution. We might consider such sacrifice of part of the physical reality to be justifiable in those cases where the critical crack configuration encompasses many bridging sites, as perhaps in a typical strength test.[4]

The problem may now be formalized by writing down a microstructure-associated stress intensity factor in terms of the familiar Greens function solution for line cracks:[8,10,11]

$$K_\mu = 0 \qquad (d_0 > c) \tag{3a}$$

$$K_\mu = -(2\psi/\pi)c^{1/2}\int_{d_0}^{c} p(x)\,d(x)/(c^2 - x^2)^{1/2} \qquad (d_0 \le c \le c^*) \tag{3b}$$

$$K_\mu = -(2\psi/\pi)c^{1/2}\int_{d_0+c-c^*}^{c} p(x)\,d(x)/(c^2 - x^2)^{1/2} \qquad (c > c^*) \tag{3c}$$

where ψ is a numerical crack geometry term ($\approx \pi^{1/2}$). At this point another major difficulty becomes apparent. We have no basis, either theoretical or experimental, for specifying *a priori* what form the closure stress function $p(x)$ must take. On the other hand, we do have some feeling from Part I, albeit limited, as to the functional form $p(u)$, where u is (one half) the crack opening displacement. Moreover, it is $p(u)$ rather than $p(x)$ which should in principle (if not readily in practice) be amenable to *independent* experimental or theoretical determination. Thus, given knowledge of the crack profile, we should be able to replace x by u as the integration variable in Eq. (3), and thereby proceed one step closer to a solution.

However, even this step involves some uncertainty, since the crack profile itself is bound to be strongly influenced by the distribution of surface tractions; i.e., $u(x)$ strictly depends on $p(x)$ (as well as on the applied loading configuration), which we have just acknowledged as an unknown. A proper treatment of the fracture mechanics in such cases leads to a nonlinear integral equation,[5] for which no analytical solutions are available. With this in mind we introduce a simplification by neglecting any effect that the tractions might have on the *shape* of the profile, yet at the same time taking due account of these tractions, via the way they modify the *net* driving force K in Eq. (1), in determining the *magnitude* of the crack opening displacements. Accordingly, we choose the familiar near-field solution for a slitlike crack in equilibrium, i.e., at $K = T_0$,[10,11]

$$u(x, c) = (\sqrt{8}\psi T_0/\pi E)(c - x)^{1/2} \tag{4}$$

where E is Young's modulus. Substitution of Eq. (4) into Eq. (3) then gives, in the approximation $d_0 \to c$ (e.g., specimens with large notches; see Section III)

$$K_\mu = 0 \qquad (d_0 > c) \tag{5a}$$

$$K_\mu = -(E/T_0)\int_0^{u(d_0,c)} p(u)\,du \qquad (d_0 \le c \le c^*) \tag{5b}$$

$$K_\mu = -(E/T_0)\int_0^{u^*} p(u)\,du \qquad (c > c^*) \tag{5c}$$

We point out that $u^* = u(d_0, c^*)$ is independent of c, so K_μ cuts off at $c \ge c^*$.

Thus by sacrificing self-consistency in our solutions, we have obtained simple working equations for evaluating the microstructure-associated stress intensity factor. We have only to specify the stress-separation function, $p(u)$.

(3) Stress-Separation Function for Interfacial Bridges

The function $p(u)$ is determined completely by the micromechanics of the ligamentary rupture process. We have indicated that we have limited information on what form this function should take. Generally, $p(u)$ must rise from zero at $u = 0$ to some maximum, and then tail off to zero again at the characteristic rupture separation u^*. There are instances in the literature where the rising portion of the curve is the all-dominant feature, e.g., as in brittle-fiber-reinforced composites where abrupt failure of the ligaments cuts off an otherwise monotonically increasing frictional restraining force.[5,6] On the other hand, there are cases where the tail dominates, as in concretes where the separation process is much more stable. Our observations on the alumina in Part I would suggest that it is the latter examples which relate more closely to the polycrystalline materials of interest here. Moreover, specific modeling of *one* of the potential separation factors alluded to in Part I, frictional pullout of interlocking grains, does indeed result in a monotonically (linearly) decreasing $p(u)$ function.[12]

Thus we are led to look for a trial stress separation function which is tail-dominated. The function we choose is

$$p(u) = p^*(1 - u/u^*)^m \qquad (0 \le u \le u^*) \tag{6}$$

where p^* and u^* are limiting values of the stress and separation, respectively, and m is an exponent. This equation is illustrated by the solid curves in Fig. 3 for three values of m: $m = 0$ is the simplistic case of a uniformly distributed stress over the bridging activity zone; $m = 1$ corresponds to the frictional pullout mechanism just mentioned;[12] $m = 2$ is the value adopted empirically for fiber concretes.[13] As we shall see, m reflects most strongly in the way that the ultimate T curve cuts off in the large crack size limit.

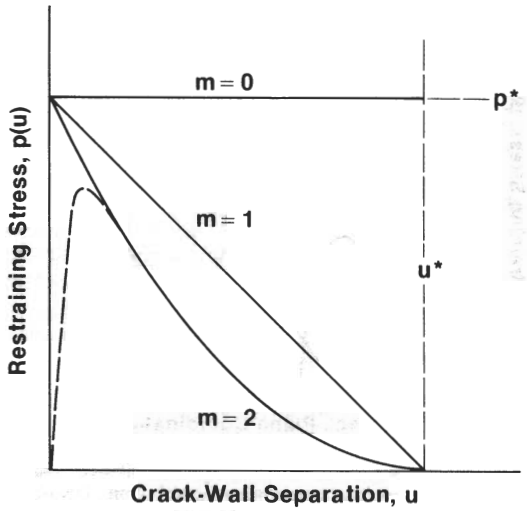

Fig. 3. Trial stress-separation function $p(u)$ for three values of exponent m in Eq. (6). Broken curve is more "realistic" function.

Note that the representation is extreme in the sense that it *totally* ignores the rising portion of $p(u)$ (cf. the broken curve in Fig. 3).

Equation (6) may now be substituted into Eq. (5) and the integration carried out to give

$$K_\mu = 0 \qquad (d_0 > c) \tag{7a}$$

$$K_\mu = -(T_\infty - T_0)\{1 - [1 - \{(c - d_0)/(c^* - d_0)\}^{1/2}]^{m+1}\} \qquad (d_0 \le c \le c^*) \tag{7b}$$

$$K_\mu = -(T_\infty - T_0) \qquad (c > c^*) \tag{7c}$$

where we have made use of Eq. (4) to eliminate $u^* = u(d_0, c^*)$ in favor of c^*, i.e.

$$c^* = d_0 + (\pi E u^*/2\sqrt{2}\,\psi T_0)^2 \tag{8}$$

and where we have defined

$$T_\infty = T_0 + Ep^*u^*/(m + 1)T_0 \tag{9}$$

to eliminate p^*.

III. Crack Resistance Curve

We are now in a position to generate the effective toughness function from Eq. (2), i.e.

$$T(c) = T_0 - K_\mu(c) \tag{10}$$

once the parameters T_0, T_∞, c^*, d_0, and m are known for any given material. Here we shall focus on the derivation of these parameters for coarse-grained alumina, leaving consideration of the crack stability (including the grain-scale discontinuities in growth referred to in Part I) to the Discussion (Section IV).

Usually, crack resistance data are obtained from test configurations which employ a starter notch, as introduced, for example, by sawcutting. The use of such a notch, in addition to providing a favorable geometry for running the crack, conveniently establishes the origin of extension at the base of the T curve. We now need to transform our coordinates, as defined in Fig. 4; we have $c = c_0 + \Delta c$, $d_0 = c_0 + d$, where c_0 is the notch length. Combining Eqs. (7) and (10) then gives

$$T(\Delta c) = T_0 \qquad (d > \Delta c) \tag{11a}$$

$$T(\Delta c) = T_\infty - (T_\infty - T_0) \times \{1 - [(\Delta c - d)/(\Delta c^* - d)]^{1/2}\}^{m+1} \qquad (d \le \Delta c \le \Delta c^*) \tag{11b}$$

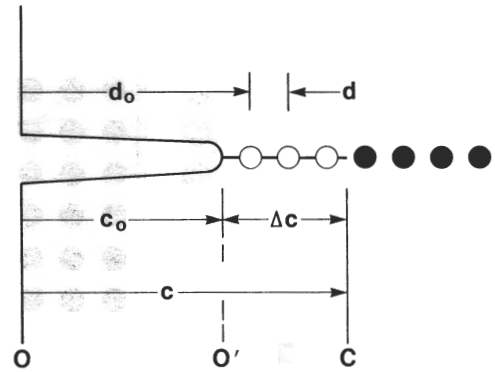

Fig. 4. Coordinates for crack system with starter notch. Effect of notch is to remove all "memory" of bridging restraints over OO', equivalent to redefining the crack origin at O'. Circles indicate bridging sites as in Fig. 1.

$$T(\Delta c) = T_\infty \qquad (\Delta c > \Delta c^*) \tag{11c}$$

Thus within the limits of the approximations used here (most notably the "small-scale zone" approximation used to derive Eq. (5)), we obtain a T curve which is geometry insensitive, i.e., independent of c_0. Note also that the steady-state bridging zone length from Eq. (8)

$$\Delta c^* = d + (\pi E u^*/2\sqrt{2}\,\psi T_0)^2 \tag{12}$$

is likewise geometry insensitive. We shall have more to say about this in Section IV. At this stage the rationale for our parameter definitions becomes apparent: T_0 and T_∞ define the lower and upper bounds, and Δc^* the spatial extent, of the T curve.

To illustrate the applicability of the formulation we examine the degree of fit of Eq. (11) to some experimental data, provided to us by M. V. Swain on a coarse-grained alumina. The material tested by Swain was of closely similar microstructure to that of the alumina used by us in Part I, i.e., reasonably large grain size (16 μm; cf. 20 μm in Part I) and nominally pure composition. He used rectangular double cantilever beam (DCB) specimens, dimensions 50 by 8 by 5 mm, notch length 11 mm, to obtain his crack data. These particular data were chosen over others in the literature because of the special precautions taken to minimize specimen end effects (see Section IV). Swain's results are plotted as the data points in Fig. 5. The theoretical fits, shown as the solid curves for fixed exponents $m = 0$, 1, and 2, were computed for trial values of $d = 50$ μm ($\approx$3 grain diameters) and $\Delta c^* = 10$ mm ($\approx$600 grain diameters) in accordance with the estimates from Part I, with T_0 and T_∞ as regression adjustables.

A word of caution is in order here. Any "goodness of fit" that we might consider evident in Fig. 5 may properly be taken as lending credence to our model. However, it should not be seen as constituting *proof* of our model. In essence, our equations contain five parameters whose values are, to a greater or lesser extent, unknown a priori. Thus, for instance, the accuracy of the fit is not sensitive to the trial value of d, but it *is* sensitive to Δc^* (reflecting the fact that the DCB data are weighted toward the region $\Delta c \gg d$). Such sensitivity to the choice of any *one* parameter inevitably contributes to the uncertainty in the *other* parameters. Consequently, despite all outward appearances in Fig. 5, we would be reluctant to assert that $m = 0$ is the "true" value of the toughness exponent.

Notwithstanding these uncertainties in the parameter determinations, we may usefully estimate the force-separation parameters p^* and u^* in Eq. (6). Thus, substituting $E = 400$ GPa, $\psi = \pi^{1/2}$ (ideal line cracks), along with the best-fit values of T_0, into Eq. (12) gives $u^* \simeq 1$ μm (independent of m). This is of the order of the crack opening displacements evident in the micrographs in Part I. Further substitution together with the regressed T_∞ values into Eq. (9) gives $p^* \simeq 25$ MPa ($m = 0$), 40 MPa

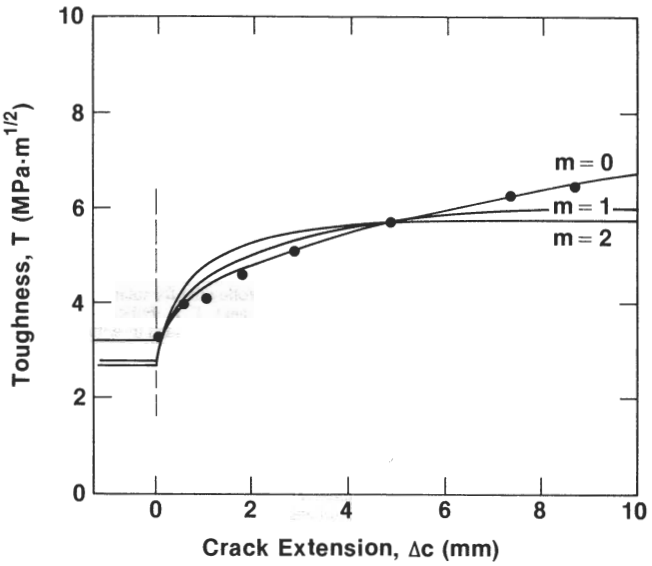

Fig. 5. Fit of Eq. (11) to double cantilever beam (DCB) toughness data on coarse-grained alumina. Fits are for $d = 50$ μm, $\Delta c^* = 10$ mm, and $m = 0$, 1, and 2, with T_0 and T_∞ as adjustables. (Data courtesy M. V. Swain.)

($m = 1$), and 55 MPa ($m = 2$). If these stress levels seem low, we may note that the composite quantity $p^*u^*/(m + 1)$, which represents the work per unit area to separate the bridges across the fracture plane (see integral in Eq. 5(*c*)), is of order 20 J·m^{-2}, i.e., comparable with typical fracture surface energies.

Finally in this section, let us note that we have yet to address the issue of crack instabilities in the *T*-curve characteristic. Recall that our analysis smoothes out all but the very first bridge discontinuity, i.e., at $c = d_0$; the data in Fig. 5 are insufficiently detailed in this region to allow any quantitative resolution of this question. We need to go to short-crack configurations. An account of the *T*-curve construction for such configurations is deferred to Section IV.

IV. Discussion

We have derived a *T*-curve (*R*-curve) model based on bridging tractions at the crack interface behind the advancing tip. The model contains several adjustable parameters, but parameters to which we may nonetheless attach physical meaning. Thus the spatial parameters c^* (Δc^*) and d, respectively, define the *range* of the T curve and the *characteristic separation* between bridging elements. The toughness parameters T_0 and T_∞ respectively define the *base crack resistance* in the absence of microstructural restraints (lower limit to T curve) and the *macroscopic crack resistance* (upper limit). Then we have the parameters m, p^*, and u^*, which determine the empirical force-separation "law" for the bridging process. These parameters, once evaluated for a given material, could be useful in structural design.

It is instructive to consider how the present treatment of the microstructural contribution to crack resistance characteristics differs from that proposed in an earlier study of indentation-strength systems.[2,3] In that study the microstructure-associated stress intensity factor K_m (cf. K_μ used in this work) was introduced in terms of an empirical grain-localized driving force at the radial crack center, in direct analogy to the (well-documented) residual-contact force field.[14,15] There, K_m was defined as a *positive* term *decreasing* with respect to crack size, with T_∞ as the reference toughness level (i.e., the level at which $K_m = 0$). Here, K_μ is defined as a *negative* (closure) term *increasing* with respect to crack size, with T_0 to the reference toughness level ($K_\mu = 0$). Conventional fracture mechanics measurements, i.e., measurements of crack size as a function of applied load, cannot in themselves distinguish between these two alternative K descriptions. It is in this context that the direct observations in Part I may be seen as critical. Moreover, the new model has its roots in a positively identifiable toughening mechanism, so taking us one step closer to a fundamental base for a priori predictions.

However, it needs to be reemphasized that the element of empiricism has not been entirely eliminated in the present treatment. There is the issue of the force-separation relation $p(u)$, which we have represented by the tail-dominated function in Eq. (6). Ideally, we would like to be able to determine $p(u)$ from first principles, but this would require a more detailed understanding of the grain bridging micromechanisms than is available at present. Only then may we hope to specify what intrinsic material properties, other than E and T_0 (see Eq. (5)), govern the toughness behavior. At that stage we may be in a position to answer some of the more pressing questions that arise in connection with observed *T*-curve trends. Thus, what is the explicit dependence of toughness on grain size, and (perhaps more intriguingly) what is it about the incorporation of a glassy grain boundary phase which so dramatically washes out the *T*-curve effect?[2,3] What role do internal microstresses play? It is with such issues that our ultimate ability to tailor superior structural ceramics must surely rest.

There are other limitations of our analysis which warrant further comment, particularly in relation to geometric effects. In our quest for an analytical solution to the fracture mechanics equations we have resorted to a questionable approximation of the crack-wall displacement profile, Eq. (4). Quite apart from the fact that this approximation is strictly justifiable only for traction-free walls, i.e., in clear violation of the very boundary conditions that we seek to incorporate into our analysis, it requires that we should not attempt to extend the description beyond the confines of the near field. Yet the results of our experimental observations in Part I show bridging activity zones of order millimeters, which is by no means an insignificant length in comparison to typical test specimen dimensions. Thus, contrary to the predictions of Eq. (11), we should not be surprised to find a strong geometry dependence in the measured *T*-curve response. Such a dependence has been observed in practice, particularly in single-edge-notched beam specimens of alumina with different starter notch lengths.[16–19] There are in fact reported instances, in fiber-reinforced cements,[20] where specimen size effects can *dominate* the intrinsic component in the *T*-curve characteristic. This is an added concern for the design engineer, whose faith in the *T*-curve construction is heavily reliant on our ability to prescribe $T(c)$ as a true material property.

Notwithstanding the above reservations, let us return to the question of crack growth discontinuities raised toward the end of Section III. It was pointed out that we need to consider short cracks, i.e., cracks smaller in length than the distance to the first bridging sites, and indeed preferably smaller than the mean bridge spacing itself. This is, of course, the domain of natural flaws. The indentation method is one way of introducing cracks of this scale, with a high degree of control, and will be the subject of a detailed quantitative analysis elsewhere.[4] For the present, we simply consider such a crack, but without residual contact stresses, subjected to a uniformly applied tensile stress, σ_a. Figure 6 is a schematic *T*-curve construction for this system, showing how the initial crack at $c_I < d$ evolves as the applied stress is increased to failure. The plot is in normalized logarithmic coordinates, to highlight the response at small c. This same plotting scheme allows for a convenient representation of the applied stress intensity factor, $K_a = \psi\sigma_a c^{1/2}$, as a family of parallel lines of slope ½ at different stress levels. The sequence of events is then as follows: (i) at loading stage 1, $K_a = K_a(\sigma_a)_1$, the crack remains stationary; (ii) at stage 2, the crack attains equilibrium at $K_a = T(c)$, and extends from an unstable state at I ($dK_a/dc > dT/dc$) to a stable state at J ($dK_a/dc < dT/dc$); (iii) on increasing the load to stage 3, the crack propagates stably through J to L up the T curve; (iv) at stage 4, a tangency condition is achieved at M, whence failure occurs. Thus our model has the capacity to account for the first crack jump discontinuity (pop-in), as well as the enhanced stability, we have come to associate with this class of material.

As a corollary of the construction in Fig. 6, note that the critical loading condition at M is not affected in any way by the initial

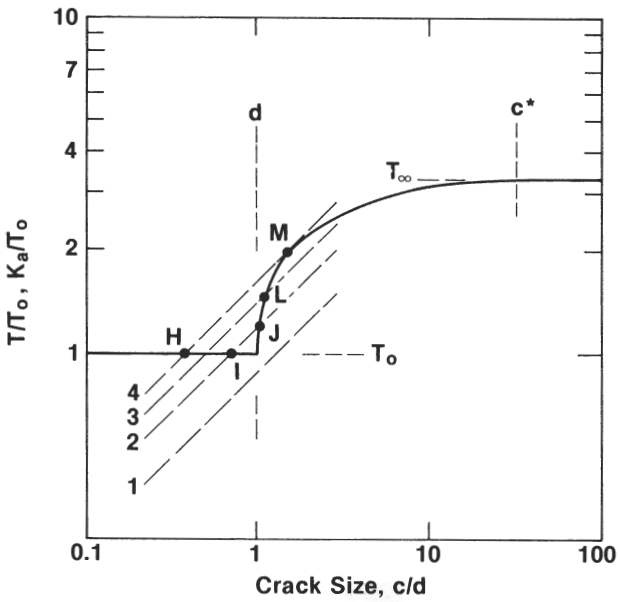

Fig. 6. T-curve construction for short crack c_I ($c_H \leq c_I \leq c_M$). Solid curve is $T(c)$ function. Inclined dashed lines $1 \rightarrow 4$ represent K_a loading lines for successively increasing values of applied stress σ_a. Crack "pops in" along IJ at stage 2 in the stressing, then progresses through JLM along curve to failure at stage 4. Note failure stress is determined exclusively by tangency condition at M, independent of initial crack size.

crack size c_I, provided this initial size falls within the range $c_H \leq c_I \leq c_M$. This explains why the strengths of specimens containing controlled flaws tend to level off at diminishing crack size (indentation load).[2] Thus we have a region of "flaw tolerance," a desirable quality from the standpoint of engineering design.

Finally, we are led to believe that the notion of crack interface bridging may have a far greater generality in the accounting of T-curve behavior in ceramics than previously suspected. We have singled out coarse-grained alumina for special study, but the earlier indentation-strength studies on a wide range of materials suggests a certain commonality in the underlying mechanisms of toughening.[2,3] At the same time, the validity of popular alternative models, particularly those founded on the hypothesis of a dispersed microcracking zone, is in serious doubt. These strong conclusions derive primarily from the direct observations described in Part I. The use of such observations as a means of identifying the responsible toughening mechanisms has been conspicuously absent in the ceramics literature. There is a clear need to develop the present treatment further, especially in regard to the bridging force-separation function. Further, the formulation should be extended to include *non*equilibrium states, where the T curve is expected to manifest itself in intriguing ways, e.g., in fatigue limits and non-unique crack velocity $v(K_a)$ functions. Our model is just the first step to a proper understanding of the toughness behavior of materials in terms of microstructural variables, which we must ultimately control if the goal of the property-tailored ceramic is ever to be realized.

Acknowledgments: The authors thank the following for their discussions on various aspects of this work: R. F. Cook, C. J. Fairbanks, E. R. Fuller, B. J. Hockey, D. B. Marshall, and P. L. Swanson. M. V. Swain kindly provided us with the data for Fig. 5 before publication.

References

[1]P. L. Swanson, C. J. Fairbanks, B. R. Lawn, Y.-W. Mai, and B. J. Hockey, "Crack-Interface Grain Bridging as a Fracture Resistance Mechanism in Ceramics: I, Experimental Study on Alumina"; this issue, preceding article.

[2]R. F. Cook, B. R. Lawn, and C. J. Fairbanks, "Microstructure-Strength Properties in Ceramics: I, Effect of Crack Size on Toughness," *J. Am. Ceram. Soc.*, **68** [11] 604–15 (1985).

[3]R. F. Cook, B. R. Lawn, and C. J. Fairbanks, "Microstructure-Strength Properties in Ceramics: II, Fatigue Relations," *J. Am. Ceram. Soc.*, **68** [11] 616–23 (1985).

[4]R. F. Cook, C. J. Fairbanks, B. R. Lawn, and Y.-W. Mai; to be published in *J. Mater. Res.*

[5]D. B. Marshall and A. G. Evans; pp. 557–68 in Proceedings of the 5th International Conference on Composite Materials. Edited by W. C. Harrigan, J. Strife, and A. K. Dhingra. Metallurgical Society of A.I.M.E., Warrendale, PA, 1985.

[6]D. B. Marshall, B. N. Cox, and A. G. Evans, "The Mechanics of Matrix Cracking in Brittle-Matrix Fiber Composites," *Acta Metall.*, **33** [11] 2013–21 (1985).

[7]D. B. Marshall and A. G. Evans; pp. 1–15 in Fracture Mechanics of Ceramics, Vol. 7. Edited by R. C. Bradt, A. G. Evans, D. P. H. Hasselman, and F. F. Lange. Plenum, New York, 1986.

[8]B. R. Lawn and T. R. Wilshaw; Ch. 3 in Fracture of Brittle Solids. Cambridge University Press, London, 1975.

[9]Y.-W. Mai and B. R. Lawn, "Crack Stability and Toughness Characteristics in Brittle Materials," *Annu. Rev. Mater. Sci.*, **16**, 415–39 (1986).

[10]G. I. Barenblatt, "The Mathematical Theory of Equilibrium Cracks in Brittle Fracture," *Adv. Appl. Mech.*, **7**, 55–129 (1962).

[11]H. Tada, P. C. Paris, and G. R. Irwin; Part III in The Stress Analysis of Cracks Handbook. Paris Productions, St. Louis, MO, 1985.

[12]A. G. Evans, A. H. Heuer, and D. L. Porter; pp. 529–56 in Fracture 1977, Vol. 1. Edited by D. M. R. Toplin. University of Waterloo Press, Ontario, Canada, 1977.

[13]R. Ballarini, S. P. Shah, and L. M. Keer, "Crack Growth in Cement-Based Composites," *Eng. Fract. Mech.*, **20** [3] 433–45 (1984).

[14]D. B. Marshall and B. R. Lawn, "Residual Stress Effects in Sharp-Contact Cracking: I. Indentation Fracture Mechanics," *J. Mater. Sci.*, **14** [9] 2001–12 (1979).

[15]B. R. Lawn, A. G. Evans, and D. B. Marshall, "Elastic/Plastic Indentation Damage in Ceramics: The Median/Radial Crack System," *J. Am. Ceram. Soc.*, **63** [9–10] 574–81 (1980).

[16]R. Knehans and R. Steinbrech, "Memory Effects of Crack Resistance During Slow Crack Growth in Notched Al_2O_3 Specimens," *J. Mater. Sci. Lett.*, **1** [8] 327–29 (1982).

[17]F. Deuler, R. Knehans, and R. Steinbrech, "Testing Methods and Crack Resistance Behavior of Al_2O_3"; to be published in *Sci. Ceram.*, Vol. 13.

[18]H. Hubner and W. Jillek, "Subcritical Crack Extension and Crack Resistance in Polycrystalline Alumina," *J. Mater. Sci.*, **12** [1] 117–25 (1977).

[19]H. Wieninger, K. Kromp, and R. F. Pabst, "Crack Resistance Curves of Alumina and Zirconia at Room Temperature," *J. Mater. Sci.*, **21** [2] 411–18 (1986).

[20]R. M. L. Foote, B. Cotterell, and Y. W. Mai; pp. 135–44 in Advances in Cement-Matrix Composites. Edited by D. M. Roy. Materials Research Society, Pennsylvania, 1980. □